A Dual-band Wireless Energy Transfer Protocol for Heterogeneous Sensor Networks Powered by RF Energy Harvesting

Prusayon Nintanavongsa*, M. Yousof Naderi†, and Kaushik R. Chowdhury†

*Department of Computer Engineering, Rajamangala University of Technology Thanyaburi, Thailand

prusayon.n@en.rmutt.ac.th

†Department of Electrical and Computer Engineering, Northeastern University, Boston, Massachusetts 02115

{naderi, krc}@ece.neu.edu

Abstract—Radio frequency (RF) energy harvesting promises to realize battery-less sensor networks by converting energy contained in electromagnetic waves into useful electrical energy. We consider a network architecture that allows heterogeneous frequency harvesting. One class of sensors harvests RF energy on the DTV band (614 MHz) while another uses the 915 MHz ISM band. We study the effective energy transfer that is achieved under these circumstances, and then design a link layer protocol called RF-HSN that optimizes the energy delivery to energy-hungry sensors with the optimal duty cycle. To the best of our knowledge, this is the first wireless energy transfer protocol for heterogeneous frequency RF energy harvesting, and through a combination of experimentation and simulation studies, we demonstrate over 59% higher duty cycle and 66% average network throughput improvement over the classical CSMA MAC protocol.

Index Terms—RF harvesting, Optimization, Medium Access Protocol, Sensor,Wireless power transfer, 915 MHz, DTV.

Fig. 1. RF energy harvesting module (915 MHz) interfaced with Mica2 sensor (a) and RF energy harvesting module (DTV band) (b)

I. INTRODUCTION

Wireless sensor networks are limited by the dependence on the on-board battery, which impacts their lifetime. Moreover regular battery replacement raises numerous risks for human personnel maintaining the network in hazardous deployment areas. The emerging area of radio frequency (RF) wireless energy is poised to alleviate some of these concerns by allowing sensors to re-charge energy storage capacitors from the incident RF radiation. We recently demonstrated this concept in a prototype that allowed a Mica2 mote to operate continuously in the 915 MHz ISM band whenever the incident signal strength was above −6 dBm [1], as shown in Figure 1(a). Moreover, developments in [2], as well as initial results circuits constructed by us (and shown in Figure 1(b)) have pointed to the possibility of RF harvesting in the digital TV band, around 614 MHz. We call these two types of sensors that can harvest in the TV band or in the 915 MHz ISM band as `Type I` and `Type II` sensors respectively. Thus, our proposed heterogeneous network is capable of harvesting from ambient radiation in the TV band, and also from controlled energy transmitters (ETs) in the ISM band. While `Type I` has the advantage of scavenging existing radiation without any nee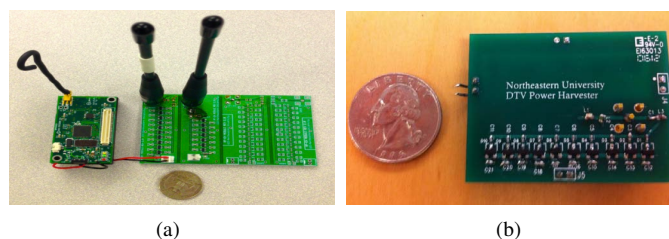d of new transmitter equipment, it is subject to the schedule followed by the TV stations, and is highly location-dependent requiring a clear line of sight. As opposed to this, `Type II` can be carefully controlled through dedicated ETs, though this introduces hardware requirements, impairs ongoing communication in the ISM band, and needs coordination among multiple ETs for effective energy transfer.

Our heterogeneous network raises several key concerns on how to manage effective charging among these sensors that harvest in multiple bands. Specifically, we address the scenarios of: (i) the primary source of wireless energy suddenly becoming unavailable, say, the TV station stops transmission owing to its established broadcast schedule (unknown to the sensors), power outages, etc. and (ii) the loss of energy signal due to device mobility, i.e., the device moves out of the transmission range of the ET. These issues pose several challenges on (i) how to sustain the communication among heterogeneous sensors when such situations occur, (ii) how to optimally deliver wireless energy to the heterogeneous sensor networks, and (iii) the challenges in aggregating the charging action of multiple sensors.

The core contributions of our work can be summarized as follows:

- We propose a link layer coordination scheme that allows sensors harvesting energy on different RF sources to interact with ETs, and rely on the latter when TV band harvesting becomes impossible. The dual-frequency harvesting and transferring scheme relaxes the reliance on a single energy source.
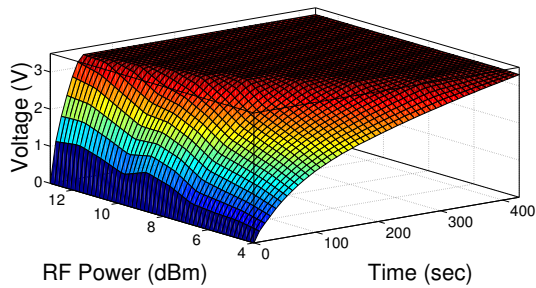
Fig. 2.   The functional representation of the charging phase [14]

Fig. 3.   Effect of capacitor sizes during capacitor discharging [14]

- We provide formulations for the optimal charging time for the energy transfer by the ETs, and combine various hardware platforms developed in prior work [1] under one operational protocol.

The rest of this paper is organized as follows: In Section II, we give the related work. Section III describes preliminary experiments used to motivate and design the RF-HSN protocol detailed in Section IV. The simulation results are presented in Section V. Finally, Section VI concludes our work.

II. RELATED WORK

RF energy harvesting mechanisms can be primarily classified as ambient RF energy harvesting and controlled RF energy harvesting. Ambient RF energy harvesting systems convert ambient RF signals such as digital TV broadcasting, cellular Base Transceiver Station (BTS), and ambient Wi-Fi radio waves into electrical energy to power RFIDs and sensor nodes. However, controlled RF energy harvesting systems use dedicated energy transmitters (i.e. wireless chargers) to generate and transfer RF waves with deliberate power intensity. Parks et al. [15] demonstrated a sensor node harvesting ambient RF energy from both digital TV and cellular radio waves that operates at a distance of 10.4 km from a 1 MW UHF television broadcast tower, and over 200 m from a cellular base transceiver station. An ambient RF energy scavenger that harvest the RF power of a TV signal through an inkjet-printed dipole antenna and a charge pump was shown in [16] and [17]. The multi-channel OFDM nature of TV signals has been exploited in [2] for powering an embedded microcontroller. Shigeta et al. [18] introduced a capacitor-leakage-aware duty cycle control method for sensor nodes powered with digital TV broadcasting signal waves, which captures the long-term and short-term fluctuations of TV signals due to the scheduled facility. Dolgov et al. [19] designed a power management system for online low power RF energy harvesting of ambient cellular waves from the BTS. Moreover, Olgun et al. [20] developed a technique to harvest ambient Wi-Fi radio waves at 2.45 GHz for powering a temperature and humidity sensor with a LCD.

Specific to the scenario of controlled RF energy harvesting, feasibility studies, prototype implementations, medium access control protocols, and duty-cycle adoptions have been explored in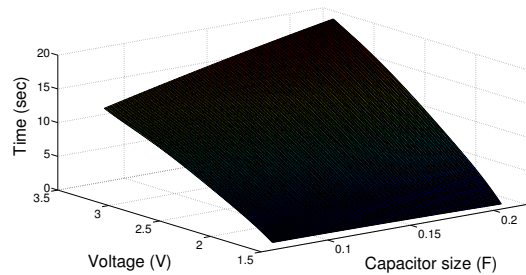 the recent past. Specifically, device characterization and cross-layer protocol design for controlled RF energy harvesting sensors are presented in [1]. Two cross-layer routing protocols that either utilize local measurements on the harvesting capability of a node (i.e., device agnostic), or employ a joint hardware-software optimization (i.e., device specific) are presented in [14]. The centralized approach in [7], and its associated analytical model in [8], are concerned with a duty-cycle based energy harvesting scheme, though our method relies on the more general purpose de-centralized control.

In [9], the authors describe conventional MAC protocols, such as the classical TDMA and variants of ALOHA under a packet deliverability metric, assuming out-of-band controlled RF energy transfer. In [22] , the authors model a CSMA-based MAC protocol with ARQ error control mechanism for energy harvesting sensor networks through an analytical framework leveraging stochastic semi-markov models. The Token-MAC protocol for RFID systems in [23] enables fair access to the medium for all tags powering by controlled RF waves requiring neither a-priori knowledge of the tags nor synchronization. The authors in [21] introduced an energy transfer mechanism and medium access technique to optimize energy delivery to desirous sensor nodes in homogeneous wireless sensor network with controlled RF energy transfer. Different from the above works, RF-HSN is the first wireless energy transfer protocol for heterogeneous RF energy harvesting sensor networks.

III. PRELIMINARY EXPERIMENTS

In our previous work [14], we conducted a set of experiments to characterize the relationship between the received power $\mathcal{P}$, the capacitor $\mathcal{C}$ that will be charged by the energy harvesting device, and the output voltage V up to which the capacitor can be charged through real measurements of our energy harvesting equipped sensor. The classical approach of using the power and voltage relationship of the capacitor, i.e., $\mathcal{V} = \mathcal{V}_o(1 - e^{\frac{t}{RC}})$ cannot be directly applied to obtain the charging time t. This is because the harvesting circuit is composed of non-linear and reactive components (Schottky diodes, inductors and capacitors) whose efficiency and reactance vary with the incident signal or power level. Several additional circuit enhancements exist, such as dynamically switching between multiple stages of the basic voltage multiplier circuit which cannot be obtained from a simple study
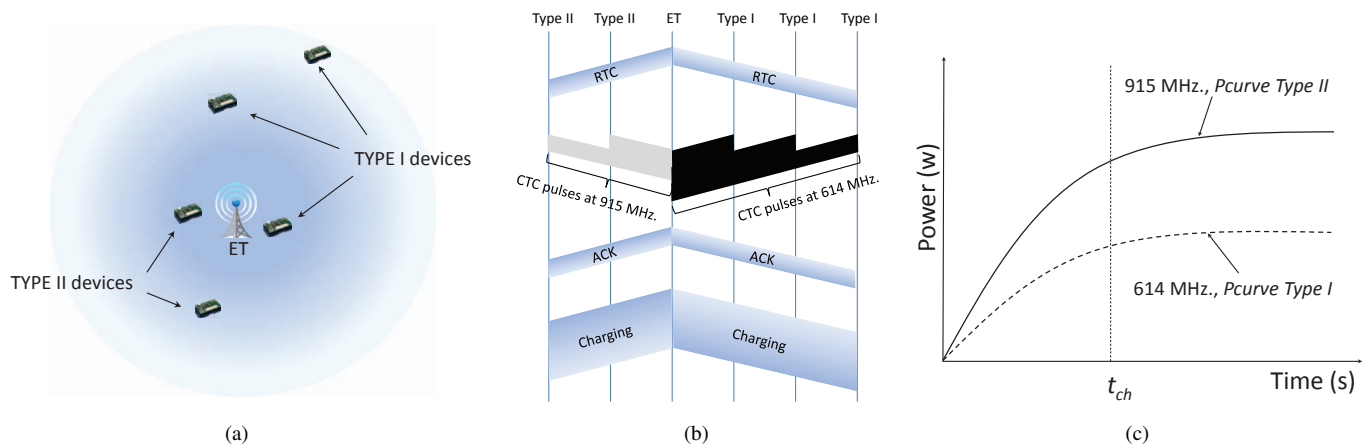
Fig. 4. Heterogeneous RF energy harvesting sensor network (a) Timing diagram for RF-HSN (b) and power curves of RF energy harvesting sensors in charging state (c)

of the circuit. Moreover, our multivariable function allows the network designer the flexibility in choosing the energy storage capacitor based on application environments.

In [14], conducted the characterization on both energy harvesting devices while using Agilent Technologies N5181A MXG RF signal generator to feed in varying signal power levels from -20 dBm to 17dBm. We also varied the storage capacitor size from 1μF to 220mF, and measured the time taken to charge to the maximum voltage output from the harvesting module (3.3V). For each capacitor size, the voltage-time curve was logged for varying input power levels. The charging characteristics of both energy harvesting circuit are derived by implementing a family of different functional approximations in MATLAB, and testing for the least square error (MSE) criterion. Figure 2 shows the functional representation of the charging phase (`Type II` device with 100 mF capacitor). It is obvious that the charging characteristic curve is not constant but varies with the level of received signal power. In other words, the characteristic of charging curve is a function of received signal power and a storage capacitor size.

Since both `Type I` and `Type II` devices employ the same load (Mica2 sensor mote), we only have to characterize the discharging characteristic once. Figure 3 shows the discharging characteristic of the device with various capacitor sizes). Note that the operational time of the devices is a function of the residual voltage and a storage capacitor size.

IV. RF-HSN PROTOCOL DESCRIPTION

Our network architecture describes `Type I` (with primary source as DTV transmissions) and `Type II` (with primary source as controllable ETs) sensors. However, we allow the `Type I` sensors to also have a secondary charging capability through dedicated ETs, which is leveraged whenever the primary source, i.e., the TV channel is inactive. Moreover, all sensors can communicate with the ET on a control channel in the 915 MHz band. We make use of standard terminology, such as *short interframe spacing* (SIFS) and *distributed interframe*

spacing (DIFS) from the 802.11 standard [5] in the following coordination scheme.

The energy transfer stage begins when the ET sends out the the Request to Charge (RTC) packet, offering to transfer wireless energy to the sensors in the network. This RTC packet can only be sent when the channel is free, i.e., when there is no ongoing data transfer or energy charging operation, and the channel lies idle for the DIFS duration. Note that RTC packet is sent out at 915 MHz, the operating frequency of Texas Instrument's CC1000 radio chip, which is equipped on Mica2 sensor mote. Consequently, both `Type I` and `Type II` devices can hear the RTC packet sent by the ET. The sensors that received the RTC then acknowledge the this packet by sending back a response, through what we call as *energy pulses*. More details on the energy pulses are given in Section IV-1. Once the ET receives the energy pulses from the responding sensors, it estimates the average power that sensors will receive during the charging process. After the charging duration is over, the ET monitors the average residual energy of the sensors, which can be determined from the discharging characteristic described in III, and sends out the RTC once the pre-set threshold is reached. The pre-set threshold (~ 2.0v in this work, as minimum operating voltage of the Mica2 is 1.8v) is set such that it allows sensors to exchange enough packets. However, it should not be set too high since the charging rate is evens out and flattens towards the upper end of the charging curve. It is best to force the network to operate within the high charging rate region.

Figure 4(a) shows a sample scenario of the heterogeneous RF energy harvesting sensor networks, i.e., when `Type I` devices find that their primary source of harvesting (DTV signal) is insufficient or, in the worst case, unavailable. In order to sustain the communication among devices, the ET needs to serve an the secondary source of energy to the `Type I` sensors primarily harvesting in the 614 MHz band. Moreover, the ET also provides the 915 MHz energy signal to `Type II` devices per its primary mode of operation.

1) Grouping of the responding sensors: The sensors that hear the RTC packet reply back with a single, constant energy pulse called Clear to Charge (CTC). Since there are two types of devices harvesting energy at different frequencies, the constant energy pulse is sent out on either $614\,\mathrm{MHz}$ or $915\,\mathrm{MHz}$, depending on the operating frequency of the harvesting module equipped, i.e., `Type I` devices respond with $614\,\mathrm{MHz}$ constant energy pulse and `Type II` devices respond with $915\,\mathrm{MHz}$ constant energy pulse. The constant energy pulse is emitted in a time slot, beginning from the instant of completion of the RTC packet, as shown in Figure 4(b). Consequently, `Type I` devices transmit constant energy pulses in the same time slot that `Type II` devices transmit their constant energy pulses. Note that there will be no interference in differentiating the band of received energy pulses at the ET since `Type I` and `Type II` devices respond to the RTC packet in different spectrum bands. Referring again to the time slot in Figure 4(b), the CTC pulses sent by `Type I` devices at $614\,\mathrm{MHz}$ is shown in black while CTC pulses sent by `Type II` devices at $915\,\mathrm{MHz}$ is shown in gray. The ET that sent the initial RTC estimates the time it needs to transmit the energy signal (charging time) based on the signal strength of the received CTC pulses on both frequencies. This arrangement of using the CTC pulses allows the sensors to be simple in design, and removes the concern of collisions in the reply packet. Unlike classical data communication, it is not important for the ET to know the required energy of each sensor. Rather, the energy requirement calculations are based on *how much* energy is needed by the two type of devices separately. We define this cumulative energy as $E_{RX}^{Type\ I}$ and $E_{RX}^{Type\ II}$, respectively, which are calculated by the RTC issuing ET from the received pulses of both frequency bands. Each slot time is $10\,\mu s$ in our work, allowing a very fast response time. The purpose of differentiating the energy requirement from the two group of devices is useful in the next stage, where an optimization function returns the optimal energy transfer with the highest duty cycle.

2) Optimization function for optimal energy delivery: The aim of the optimization formulation is to maximize the energy transfer $E_{RX}^{Max} = E_{RX}^{Type\ I} + E_{RX}^{Type\ II}$ to the coverage area of the ET with the highest duty cycle. The energy transferred by the RF signal at each frequency is the time integral of the power (charging characteristic) curve at the corresponding frequency. Note that the power curve is a function of the received signal strength (RSS) and the charging time. Thus, the useful components that need to be maximized are two terms of (2), which give the total energy transfer to both `Type I` and `Type II` devices.

$$Given: Pcurve_I(RSS_I, t_{ch}),\ Pcurve_{II}(RSS_{II}, t_{ch})$$
$$To\ find: t_{ch} \tag{1}$$
$$To\ Maximize:$$
$$E_{RX}^{Max} = \int_{t_{ch}} Pcurve_I(RSS_I, t_{ch})\mathrm{d}t$$
$$+ \int_{t_{ch}} Pcurve_{II}(RSS_{II}, t_{ch})\mathrm{d}t \tag{2}$$

$$Subject\ to:$$
$$\frac{d(Pcurve_I(RSS_I, t_{ch}))}{\mathrm{d}t} + \frac{d(Pcurve_{II}(RSS_{II}, t_{ch}))}{\mathrm{d}t}$$
$$- \frac{d(Pdischarge(t_{ch}))}{\mathrm{d}t}\ \ is\ maximum \tag{3}$$
$$\int_{t_{ch}} Pcurve_I(RSS_I, t_{ch})\mathrm{d}t > E_{min_I} \tag{4}$$
$$\int_{t_{ch}} Pcurve_{II}(RSS_{II}, t_{ch})\mathrm{d}t > E_{min_{II}} \tag{5}$$

The aim of this optimization framework is to maximize area under the devices' power curves, subject to several constraints which are explained below:

- The sum of derivatives of power curves of `Type I`, `Type II` devices, and the discharging curve, evaluated at the charging time $t = t_{ch}$ is maximum. In other words, the aggregate rate of charging of both `Type I` and `Type II` devices, subtracted by the discharging rate, are at its maximum. This put a constraint on achieving the highest duty cycle.
- The amount of energy transfer to `Type I` and `Type II` devices has to be larger than the lowest amount of energy required for `Type I` and `Type II` devices to be in the operational state, respectively.

With the resulting dual-frequency wireless energy transfer, both groups of devices can be simultaneously active. The final part of this stage involves letting both `Type I` and `Type II` devices know that they are about to enter the charging state through an Acknowledgement (ACK) packet. This packet provides both types of devices the expected charging time and hence, the following inactive time, according to the optimization results. After a short SIFS wait period following the ACK, the ET begin its transmission. Consequently, the ET starts to deliver the energy to sensors at different frequencies, that is, $614\,\mathrm{MHz}$ charging energy signal for `Type I` devices and $915\,\mathrm{MHz}$ charging energy signal for `Type II` devices, respectively. In case of loss of the RTC packet due to packet collision or bad channel conditions, the contention windows are re-set to the minimum width, thereby initiating an immediate subsequent retry.

V. SIMULATION RESULTS

In this section, we thoroughly evaluate our proposed protocol using our custom simulator, developed in MATLAB. We observe the behavior of RF-HSN protocol with respect to difference in average received power of `Type I` and `Type II` devices. This simulation setup represents the scenario described in I, i.e., when `Type I` find that their primary source of harvesting is insufficient or unavailable. The simulation parameters are set as follows: The energy harvesting modules parameters are from [1]. We model the ET on the Powercaster transmitter [4], which is capable of transmitting continuous waves (CW) modulation at $3\,\mathrm{W}$ EIRP. However, we impose an additional feature on the ET requirement, that is, the ability to emit the CW modulation at $614\,\mathrm{MHz}$ and $915\,\mathrm{MHz}$, simultaneously. The operational characteristics of the sensor, such as energy spent in transmission, reception, idle listening, channel

bandwidth, etc. are from MICA2 specifications [13]. Unless specifically stated, 10 sensor nodes, 5 of each type, and 1 ET are deployed uniformly at random in 40 x 40 m^2 grid. Type II devices are randomly placed such that the average received power is measured $12\,\mathrm{dBm}$. On the contrary, the placement of Type I devices are randomly chosen to have various average received power, ranging from $4\,\mathrm{dBm}$ to $12\,\mathrm{dBm}$. The default packet size is 50 Bytes and the sender/receiver pairs are chosen randomly from Type I device to Type II groups. We compare the proposed RF-HSN protocol with the modified unslotted CSMA. RF-HSN features the energy delivery optimization by dynamically adjusting the charging level (hence, the charging duration), with specific constraints, in order to achieve an optimal energy delivery. The unslotted CSMA modified from the description in [6] provides the base case and reference protocol for comparison. The sensors are always charged to the maximum level, at 3.3V and we assume saturated condition wherein sensors always have a packet to transmit.

A. Impact on average energy harvesting rate

Here, we investigate the effect of difference in average received power for the Type I and Type II devices depending on average energy harvesting rate. Figure 5 shows the effect of the average received power of Type I devices for both RF-HSN and modified CSMA protocols. As stated earlier, the placement of Type II devices is fixed with the average received power of $12\,\mathrm{dBm}$ while Type I devices are deployed with varied averaged received power, ranging from $4\,\mathrm{dBm}$ to $12\,\mathrm{dBm}$. It is not surprising that both RF-HSN and the modified CSMA deliver monotonically increasing average energy harvesting rate with increasing received power of Type I devices. However, the benefit of energy delivery optimization, incorporated in RF-HSN, greatly improves the average energy harvesting rate. The improvement is over 59% when the average received power of Type I devices is at $4\,\mathrm{dBm}$ and tapered down to 20% when the average received power of Type I devices is equal to that of Type II devices, at $12\,\mathrm{dBm}$. The reduction in an improvement is a result of steeper and less deflected power curves of both Type I and Type II devices in higher received power regime, which gives less room for optimization of RF-HSN protocol.

B. Impact on duty cycle of the network

The impact of average received power of Type I devices on the duty cycle is shown in Figure 6. It is obvious that RF-HSN yields higher duty cycle throughout the range. When the average received power of Type I devices is at $4\,\mathrm{dBm}$, RF-HSN yields 7.51% duty cycle while only 3.86% duty cycle is achieved by the modified CSMA, over 94.66% higher in duty cycle. The duty cycle plot also resembles to that of the average energy harvesting rate plot, that is, the duty cycle gain decreases as average received power of Type I devices increases. At $12\,\mathrm{dBm}$ of average received power of Type I devices, RF-HSN yields 34.46% higher duty cycle than the modified CSMA.
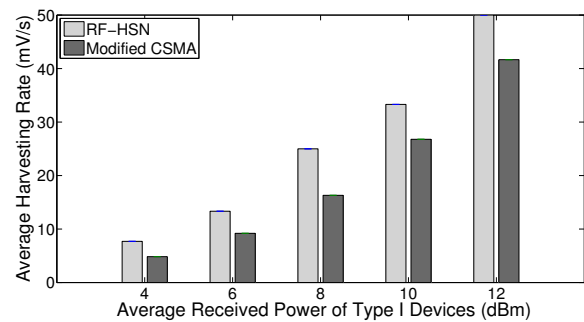

Fig. 5. Effect of the average received power of Type I devices on average energy harvesting rate
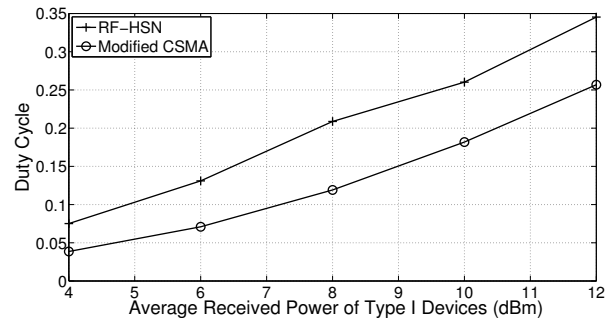

Fig. 6. Effect of the average received power of Type I devices on duty cycle

C. Impact on average packet delay

One of the major concerns of RF energy harvesting sensor networks is the inactive period of the sensors due to energy replenishing (charging process). It is crucial to investigate the average packet latency of the proposed protocol, especially when time-sensitive applications are involved. Figure 7 shows the impact on average packet delay against various average received power of Type I devices, and complements the duty cycle plot shown earlier. Since the duty cycle is defined as the sensor's active period over the sum of sensor's active and inactive period, it does not capture the information about an absolute sensor's inactive time, but rather a relative active time. It is clear that RF-HSN offers a considerably less average packet delay when the average received power of Type I devices is at $4\,\mathrm{dBm}$, only $13\,\mathrm{s}$ (RF-HSN) compared to $310\,\mathrm{s}$ (modified CSMA). Moreover, RF-HSN is not susceptible to the fluctuation of average received power of Type I devices. As shown in Figure 7, the average packet delay of RF-HSN experiences considerably less fluctuation when compared to that of modified CSMA.

D. Impact on network throughput

Figure 8 depicts the network throughput when average received power of Type I devices is varied from $4\,\mathrm{dBm}$ to $12\,\mathrm{dBm}$. Similar to the earlier case, RF-HSN outperforms the modified CSMA in terms of network throughput throughout the range. On average, RF-HSN yields approximately 66% higher network throughput than the modified CSMA.
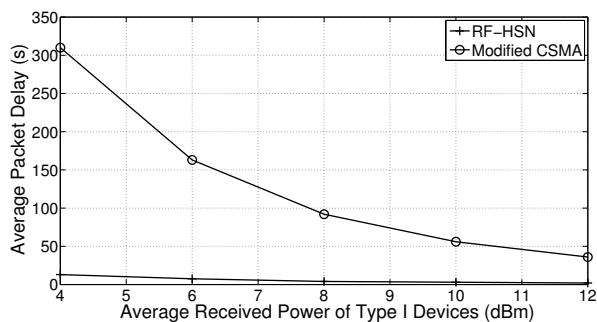
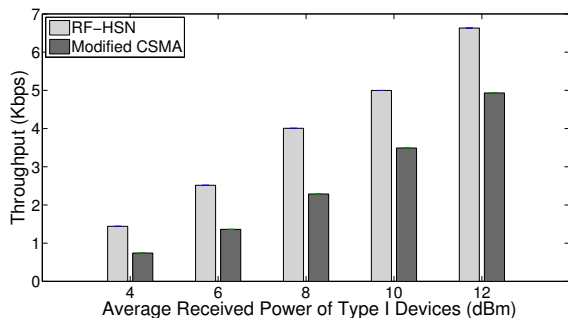Fig. 7. Effect of the average received power of `Type I` devices on average packet delay

Fig. 8. Effect of the average received power of `Type I` devices on average network throughput

VI. CONCLUSIONS

The RF-HSN protocol defines new metrics in wireless energy transfer for heterogeneous RF energy harvesting sensor networks through wireless energy delivery optimization. This optimization ensures the optimal energy delivery with the highest duty cycle. Our new architecture for RF energy harvesting will allow seamless interoperability among heterogeneous sensors, harvesting at different RF frequency sources, especially leveraging the large ambient energy present in the DTV band. Our previous work, on the RF energy harvesting platform fabrication and characterization of their characteristics, is used to shape the deign goals of the RF-HSN protocol under rigid experimental constrains. Simulation results reveals that RF-HSN largely outperforms the modified CSMA. The higher duty cycle, together with considerably lower average packet latency, make the RF-HSN protocol a preferred choice for heterogeneous RF energy harvesting sensor networks.

REFERENCES

[1] P. Nintanavongsa, U. Muncuk, D. R. Lewis, and K. R. Chowdhury, Design Optimization and Implementation for RF Energy Harvesting Circuits. *IEEE Journal on Emerging and Selected Topics in Circuits and Systems*, vol. 2, no. 1, pp. 24–33, Mar. 2012.

[2] R. J. Vyas, B. B. Cook, Y. Kawahara, and M. M. Tentzeris, E-WEHP: A Batteryless Embedded Sensor-Platform Wirelessly Powered From Ambient Digital-TV Signals. *IEEE Transactions on Microwave Theory and Techniques*, vol. 61, no. 6, pp. 2491–2505, Jun. 2013.

[3] C. M. Vigorito, D. Ganesan, and A. G. Bart, Adaptive Control of Duty Cycling in Energy-Harvesting Wireless Sensor Networks. *Proc. of IEEE SECON*, pp. 21–30, Jun. 2007.

[4] Powercast Corporation, Lifetime Power Evaluation and Development Kit. [Online] http://www.powercastco.com/products/development-kits/

[5] IEEE 802.11, Wireless LAN Medium Access Control (MAC) and Physical Layer (PHY) Specification. 1999.

[6] Z. A. Eu, H.P. Tan, and W. K. G. Seah, Design and performance analysis of MAC Schemes for Wireless Sensor Networks Powered by Ambient Energy Harvesting. *Ad Hoc Networks*, vol. 9, no. 3, pp. 300–323, 2011.

[7] J. Kim and J. W. Lee, Energy Adaptive MAC Protocol for Wireless Sensor Networks with RF Energy Transfer. *Proc. of IEEE Intl. Conference on Ubiquitous and Future Networks (ICUFN)*, pp. 89–94, 2011.

[8] J. Kim and J. W. Lee, Performance Analysis of the Energy Adaptive MAC Protocol for Wireless Sensor Networks with RF Energy Transfer. *Proc. of IEEE Intl. Coverage and Transmission Conference (ICTC)*, pp. 14–19, 2011.

[9] F. Iannello, O. Simeone, and U. Spagnolini, Medium Access Control Protocols for Wireless Sensor Networks with Energy Harvesting. *IEEE Transactions on Communications*, vol. 60, no.5, pp. 1381–1389, May. 2012.

[10] M.K. Watfa, H. AI-Hassanieh, S. Selman, Multi-hop wireless energy transfer in WSNs. *IEEE Communication Letter*, vol. 15, no. 12, pp. 1255–1277, Oct. 2011.

[11] A. Karalis, J. D. Joannopoulos, and M. Soljacic, Efficient wireless nonradiative mid-range energy transfer. *Annals of Physics*, vol. 323, no. 1, pp. 34–48, Jan. 2008.

[12] J. Curty, M. Declercq, C. Dehollain, N. Joehl, Design and Optimization of Passive UHF RFID Systems, Springer, 2007.

[13] Crossbow Technology, Inc. [Online] http://www.xbow.com/

[14] P. Nintanavongsa, R. Doost, M. Di Felice, and K. R. Chowdhury, Device characterization and cross-layer protocol design for RF energy harvesting sensors. *Elsevier Journal of Pervasive and Mobile Computing*, vol. 9, no. 1, February 2013.

[15] A. Parks, A. Sample, Y. Zhao, and J. R. Smith, A wireless sensing platform utilizing ambient RF energy. *IEEE Topical Meeting on Wireless Sensors and Sensor Networks (WiSNET)*, Austin, TX, Jan 2013.

[16] H. Nishimoto, Y. Kawahara, and T. Asami, Prototype implementation of wireless sensor network using TV broadcast RF energy harvesting. *12th ACM international conference adjunct papers on Ubiquitous computing*, pp. 373–374, Copenhagen, Denmark, Sep 2010.

[17] R. Vyas, H. Nishimoto, M. Tentzeris, Y. Kawahara, and T. Asami, A battery-less, energy harvesting device for long range scavenging of wireless power from terrestrial TV broadcasts. *IEEE MTT-S International Microwave Symposium Digest (MTT)*, Montreal, Canada, June 2012.

[18] R. Shigeta, T. Sasaki, D. Minh Quan, Y. Kawahara, R. J. Vyas, M. M. Tentzeris, and T. Asami, Ambient-RF-Energy-Harvesting Sensor Device with Capacitor-Leakage-Aware Duty Cycle Control. *IEEE Sensors Journal*, pp. 1–10, July 2013.

[19] A. Dolgov, R. Zane, and Z. Popovic, Power management system for online low power RF energy harvesting optimization. *IEEE Transactions on Circuits and Systems I: Regular Papers*, vol. 57, no. 7, pp. 1802–1811, July 2010.

[20] U. Olgun, C.-C. Chen, and J. Volakis, Design of an efficient ambient Wi-Fi energy harvesting system. *IET Microwaves, Antennas Propagation*, vol. 6, no. 11, pp. 1200–1206, Aug 2012.

[21] P. Nintanavongsa, M.Y. Naderi, and K. R. Chowdhury, Medium Access Control Protocol Design for Sensors Powered by Wireless Energy Transfer. *Proc. of IEEE International Conference on Computer Communications (INFOCOM)*, pp. 150–154 , April 2013.

[22] M.Y. Naderi, S. Basagni, and K.R. Chowdhury, Modeling the Residual Energy and Lifetime of Energy Harvesting Sensor Nodes. *Proc. of IEEE Global Telecommunications Conference (GLOBECOM)*, pp. 3394–3400, Dec. 2012.

[23] L. Chen, I. Demirkol, and W. Heinzelman, Token-MAC: A Fair MAC Protocol for Passive RFID Systems. *Proc. of IEEE Global Telecommunications Conference (GLOBECOM)*, pp. 1–5, Dec. 2011.